Real time groove characterization combining partial least squares and SVR strategies: application to eddy current testing

IOP Conf. Series: Journal of Physics: Conf. Series **904** (2017) 012017 doi:10.1088/1742-6596/904/1/012017

Real time groove characterization combining partial least squares and SVR strategies: application to eddy current testing

S Ahmed[1], M Salucci[2], R Miorelli[1], N Anselmi[2], G Oliveri[2], P Calmon[1], C Reboud[1] and A Massa[2,3]

[1]CEA LIST, Centre de Saclay, F- 91191 Gif-sur-Yvette, France
[2]ELEDIA Research Center (ELEDIA@UniTN - University of Trento)
Via Sommarive 9, I-38123 Trento, Italy
[3]ELEDIA Research Center (ELEDIA@L2S - UMR8506)
3 rue Joliot-Curie 91192 Gif-sur-Yvette, France
E-mail: andrea.massa@l2s.centralesupelec.fr

Abstract. A quasi real-time inversion strategy is presented for groove characterization of a conductive non-ferromagnetic tube structure by exploiting eddy current testing (ECT) signal. Inversion problem has been formulated by non-iterative Learning-by-Examples (LBE) strategy. Within the framework of LBE, an efficient training strategy has been adopted with the combination of feature extraction and a customized version of output space filling (OSF) adaptive sampling in order to get optimal training set during *offline* phase. Partial Least Squares (PLS) and Support Vector Regression (SVR) have been exploited for feature extraction and prediction technique respectively to have robust and accurate real time inversion during *online* phase.

1. Introduction

Nowadays non-invasive inspection through non-destructive testing and evaluation (NDT-NDE) is becoming very popular area of research for different applications. Among different electromagnetic NDT (E-NDT) methods, lower frequency eddy current testing (ECT) is widely used for the assessment of the integrity of the structure under test (SUT) by means of defect or crack detection, localization and characterization. Within this context, the necessity of quicker and reliable inverse solutions becomes the main priority in many industrial applications. In general, inversion strategy can be classified into iterative and non-iterative methods. Standard iterative approaches based on deterministic or stochastic algorithms [1]-[4] can be too cumbersome due to the solution of several hundred up to thousands forward problems in order to minimize a suitable cost function. This aspect can be computationally expensive and time demanding tasks. Alternatively, non-iterative techniques have recently shown to be able to address quite successfully inversion issues [5]-[6]. Nevertheless, due to the limitations on certain probe assessment, they cannot be applied directly to any kind of NDE problems. Among the non-iterative approaches, kernel-based strategies [7]-[8] have been presented in the past years while Learning-by-Examples (LBE) strategies have been proposed recently for quasi real time inverse solution [9]-[10]. Following the presented work at [9]-[10] LBE strategy can be formulated in two phases. At the preliminary *offline* phase, a fast and accurate model is built by generating a training set of input-output (I/O) pairs. During the second phase (*online* phase), the developed model from *offline* phase is used to predict the output associated to an unknown test sample. The performance of different LBE strategies depends on the particular choice of the training set generation in terms of samples selection in parameter space and features extraction in ECT signal space. Towards this end, this work describes an adaptive-sampling strategy which combines Partial Least Squares (PLS) [11] feature extraction and output space filling (OSF) sampling [8]. This strategy aims to uniformly explore the extracted feature space to have enough information for training set generation. Finally a set of Support Vector Regressors (SVR) [12] are exploited for accurate and quasi

real-time inversion for groove characterization within a tube structure. Moreover, the robustness of the proposed *PLS-OSF/SVR* strategy is also evaluated for noisy test case based on numerical benchmark problem.

2. Mathematical formulation of forward and inverse problem

Let us consider a 2D axisymmetric configuration made by conductive tube having conductivity σ, relative permittivity $\varepsilon_r = 1$ and permeability $\mu_r = 1$ (Fig. 1). The tube is inspected by two coils which are excited by a time-harmonic current. The coils centred at $x = 0$ and $z = 0$ are working in differential mode and moving along the tube y axis. The tube is effected by a single axisymmetric groove that occupies a volumetric region Ω within the *SUT* (i.e., $\sigma(\mathbf{r}) \neq \sigma \quad \forall \mathbf{r} \in \Omega$ - Fig. 1). The impedance variation measured by the coils at the *k*-th scanning position with respect to the flawless scenario ($k = 1,...,K$) is given by [13]

$$\Psi_k = -\frac{1}{I^2}\int_{\Omega} \mathbf{E}^{inc}(\mathbf{r}\,|\,\mathbf{r}_k)\cdot\boldsymbol{\rho}(\mathbf{r}\,|\,\mathbf{r}_k)d\mathbf{r} \tag{1}$$

I is the current flowing inside the coil while $\mathbf{E}^{inc}(\mathbf{r}\,|\,\mathbf{r}_k)$ is the incident field generated at position $\mathbf{r}$ in the unflawed tube ($\mathbf{r}_k = y_k$ represents the *k*-th coil position along the tube). $\boldsymbol{\rho}(\mathbf{r}\,|\,\mathbf{r}_k)$ represents the unknown induced current dipole density, which models the presence of the groove and is related to the total field, $\mathbf{E}^{tot}(\mathbf{r}\,|\,\mathbf{r}_k)$ that can be expressed by

$$\boldsymbol{\rho}(\mathbf{r}\,|\,\mathbf{r}_k) = [\sigma(\mathbf{r}) - \sigma]\mathbf{E}^{tot}(\mathbf{r}\,|\,\mathbf{r}_k). \tag{2}$$

Let us model the region Ω of the groove by a finite set of *Q*=3 descriptors $\underline{p} = (y_c, d_c, w_c)$. h_c and w_c are the height and width of the groove placing at y_c position along the tube axis with an angular extension of 360^o (Fig. 1).

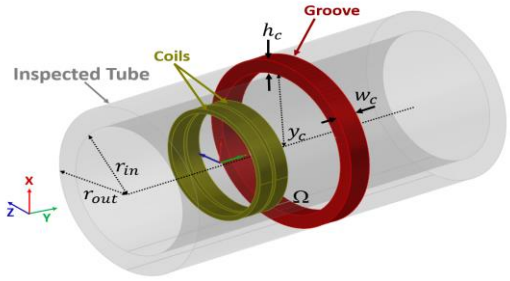

Figure 1. Tube geometry of the considered ECT problem.

Eq. (1) can be expressed in implicit form by means of the forward operator $\Phi\{.\}$ by $\Psi_k = \Phi\{\mathbf{r}_k, \underline{p}\}$, for $k = 1,...,K$. CIVA [14] simulator is utilized for generating ECT signals associated to the coils differential impedance variation. The (unknown) inverse operator $\Phi^{-1}\{.\}$ allows to estimate the (unknown) groove parameters [i.e., $\underline{\tilde{p}} = (\tilde{p}_q; q = 1,...,Q)$] by exploiting the information collected through ECT signals. Within the framework of LBE a regression problem is formulated for the estimation of $\Phi^{-1}\{.\}$ by suitably processing a set of *N* I/O pairs [i.e., a training set, $D_N = \left\{\left(\underline{\Psi}^{(n)}; \underline{p}^{(n)}\right); n = 1,...,N\right\}$]. Due to the complex nature of the ECT signals, the *n*-th input is represented by the set $\underline{\Psi}^{(n)} = \left(\Re\left\{\Psi_k^{(n)}\right\}, \Im\left\{\Psi_k^{(n)}\right\}; k = 1,...,K\right)$ of $F = 2K$ measured features associated to the *n*-th output $\underline{p}^{(n)} = \left(p_q^{(n)}; q = 1,...,Q\right)$. The main goal of the proposed solution is to apply PLS feature extraction on *F* measured features to reduce the dimension of actual ECT feature space and perform adaptive sampling

directly in the extracted feature space in order to retrieve the lowest N number of training samples during *offline* phase. This provides an exhaustive representation of the I/O relationship for optimal and almost real time inverse solution during *online* phase. The following steps describe the iterative procedure in order to adaptively select samples during the *offline* phase.

i. ***Initialization***- Generate $N = N_0$ number of initial samples by using a uniform grid sampling within the groove parameter space (i.e., $\underline{p}^{(n)}, n = 1,..., N$). $N_{\max}$ is the maximum desired/feasible training size (i.e., $N_0 < N_{\max}$). By using $\Phi\{.\}$ generate ECT coil signals and fill the $(N \times F)$ feature matrix $\underline{\underline{\Psi}}$ whose n-th row is represented by $\underline{\Psi}^{(n)}$. A matrix of groove parameters, $\underline{\underline{p}}$ having $(N \times Q)$ dimension is formed where $\underline{p}^{(n)}$ is the n-th row of $\underline{\underline{p}}$.

ii. ***Feature Extraction***- Build the $(N \times F)$ matrix $\underline{\underline{\Psi}}^T$ by subtracting each f-th column of $\underline{\underline{\Psi}}$ $(f = 1,..., F)$ from its mean value, μ_f and compute the $(N \times Q)$ matrix $\underline{\underline{p}}^T$ by subtracting each q-th column of $\underline{\underline{p}}$ $(q = 1,..., Q)$ from its mean value μ_p. Apply the *PLS* algorithm to linearly decompose $\underline{\underline{\Psi}}^T$ and $\underline{\underline{p}}^T$ as follows

$$\begin{aligned} \underline{\underline{\Psi}}^T &= \underline{\underline{T}} \times \underline{\underline{S}} + \underline{\underline{Y}} \\ \underline{\underline{p}}^T &= \underline{\underline{U}} \times \underline{\underline{Z}} + \underline{\underline{G}} \end{aligned}. \qquad (3)$$

In Eq. (3) $\underline{\underline{T}} = \left(\underline{T}^{(n)}; n = 1,...,N\right)$ is the $(N \times J)$ matrix of Ψ-scores [$\underline{T}^{(n)} = \left(T_j^{(n)}; j = 1,...,J\right)$]. It is obtained from $\underline{\underline{\Psi}}^T$ through the $(F \times J)$ weight matrix $\underline{\underline{W}}$ (i.e., $\underline{\underline{T}} = \underline{\underline{\Psi}}^T \times \underline{\underline{W}}$). J is the number of extracted features ($J < F$). $\underline{\underline{Y}}$ and $\underline{\underline{G}}$ contain the $(N \times F)$ and $(N \times Q)$ residuals of the linear decomposition while $\underline{\underline{S}}$ and $\underline{\underline{Z}}$ are the $(J \times F)$ and $(J \times Q)$ matrices of loadings. The decomposition in Eq. (3) is aimed at maximizing the covariance between the corresponding columns of $\underline{\underline{T}}$ [i.e., $\left(\overline{T}_j; j = 1,...,J\right)$] and of the $(N \times J)$ matrix of p-scores $\underline{\underline{U}}$ [i.e., $\left(\overline{U}_j; j = 1,...,J\right)$]. This guarantees all the information about the ECT signal embedded inside $\underline{\underline{\Psi}}^T$ (i.e., inside $\underline{\underline{\Psi}}$) is compressed into $\underline{\underline{T}}$. Then an initial training set $\hat{D}_N = \left\{\left(\underline{T}^{(n)}; \underline{p}^{(n)}\right); n = 1,..., N\right\}$ is formed.

iii. ***Adaptive Sampling***- By using Latin Hypercube Sampling (*LHS*) select V candidate samples within the parameter space by $\underline{p}_{cand}^{(v)} = \left(p_{cand,q}^{(v)}; q = 1,..., Q\right), v = 1,..., V$. An estimation of the J-dimensional set of extracted features corresponding to each v-th candidate, $\underline{\tilde{T}}_{cand}^{(v)}$ is retrieved by applying a multi-dimensional linear interpolator on $\hat{D}_N$. Select the candidate sample $v = v^*$ through maximizing the minimum distance with the $\underline{T}^{(n)}$ sets in $\hat{D}_N$ [i.e., $\underline{\tilde{T}}_{cand}^{(v^*)} = \arg\left(\max_v \left\{\min_n d_{vn}\right\}\right)$]. d_{vn} is the Euclidean distance between $\underline{\tilde{T}}_{cand}^{(v)}$ ($v = 1,..., V$) and $\underline{T}^{(n)}$ ($n = 1,..., N$) [i.e., $d_{vn} = \sqrt{\sum_{j=1}^{J} \left(\tilde{T}_{cand,j}^{(v)} - T_j^{(n)}\right)^2}$]. The set of F measured features associated to the selected sample $\underline{\Psi}_{cand}^{(v^*)} = \left(\Re\left\{\Psi_{cand,k}^{(v^*)}\right\}, \Im\left\{\Psi_{cand,k}^{(v^*)}\right\}; k = 1,...,K\right)$ is computed by utilizing $\Phi\{.\}$. Finally, the set of extracted features is obtained by

$$\underline{T}_{cand}^{(v^*)} = \left(\underline{\Psi}_{cand}^{(v^*)}\right)^T \times \underline{\underline{W}} \qquad (4)$$

where $\left(\underline{\Psi}_{cand}^{(v^*)}\right)^T$ is obtained by subtracting each f-th element of $\underline{\Psi}_{cand}^{(v^*)}$ ($f=1,...,F$) from its mean value μ_f. Finally, updated the training set with $\hat{D}_{N+1}=\hat{D}_N \cup \left\{\underline{T}_{cand}^{(v^*)}; \underline{p}_{cand}^{(v^*)}\right\}$ and update $N=N+1$. This is also known as OSF sampling (i.e., candidate parameters are chosen such that features are uniformly distributed in the feature space).

iv. ***Stop Criterion***- Stop adding new training samples for $N=N_{\max}$. Otherwise, repeat from Step iii.

An ε-*SVR* is trained for each q-th parameter ($q=1,...,Q$) of the groove, by exploiting the corresponding q-th set of I/O pairs $\hat{D}_{N,q}=\left\{\left(\underline{T}^{(n)}; p_q^{(n)}\right); n=1,...,N\right\}$ on the generated training set. Moreover, a test set $\underline{\Psi}_{test}$ of F measured features associated to a previously-unseen groove parameter configuration $\underline{p}_{test}$ is projected through $\underline{\underline{W}}$ into the J-dimensional *PLS*-extracted features space [i.e., $\underline{T}_{test}=\underline{\Psi}_{test}^T\times\underline{\underline{W}}$. $\underline{\Psi}_{test}^T$ is obtained by subtracting each f-th element of $\underline{\Psi}_{test}$ ($f=1,...,F$) from its mean value μ_f]. Finally, $\underline{T}_{test}$ is given as input to the q-th *SVR* in order to estimate the q-th parameter of the groove, $\tilde{p}_{test,q}$ for $q=1,...,Q$.

3. Numerical validation

Let us consider a cylindrical metal tube (Fig. 1) of height by $(r_{out}-r_{in})=1.27$ mm and $\sigma=1.0$ MS/m. Two axial current coils are working at 100 kHz in differential mode. The tube is effected by an external full groove ($\sigma(\mathbf{r})=0$ S/m, $\mathbf{r}\in\Omega$) located at $y_c=23.75$ mm with fixed angular extension 360^o. A fast metamodel is used to compute ECT signals of the coils over $K=K_x\times K_y=1\times 73=73$ probing locations with 0.2 mm spacing on *y* axis. The groove has variable height and width within the range $h_c\in[0.0635,\ 1.061]$mm, $w_c\in[1.0,\ 3.0]$ mm respectively (i.e., $Q=2$). $N_0=9$ samples are used to initialize the sampling loop while *J=4* features are extracted from $F=2K=2\times 73=146$ actual measured features. $V=100$ candidate samples are generated for each iterative step until $N=N_{\max}=49$ is obtained. Figure 2(*a*) shows the location of the sampling points in the of feature space (for graphical illustration, the resultant extracted feature space is shown for *J=2*). In Fig. 2(*b*), the sampling points have been mapped into groove parameter space for N_0 initial and the successive $(N_{\max}-N_0)$ samples.

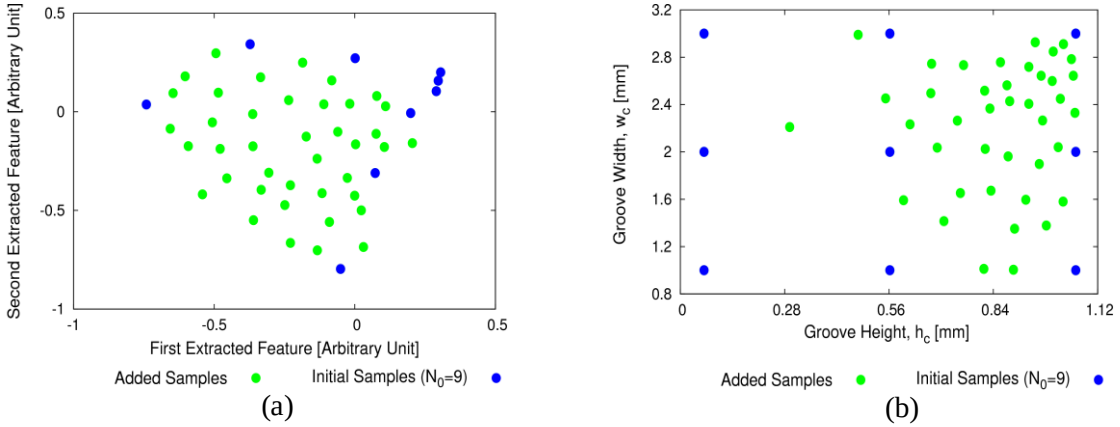

(a) (b)

Figure 2. Training samples locations mapped on (*a*) the feature space and (*b*) the parameter space for *J*=2, N_0=9, $N_{\max}$=49.

A set of $M=1000$ previously-unseen test configurations (ECT signals) associated to randomly selected groove parameters has been generated. The robustness of the *PLS-OSF/SVR* schema is

evaluated on the M test samples in presence of Additive White Gaussian Noise (AWGN). AWGN has been imposed by $SNR = [10, 20, 30, 40]$ dB according the definition mentioned in [10]. To access the performance on the prediction, normalized mean error, $NME_{p_q} = \frac{1}{M}\left(\sum_{m=1}^{M} | p_{test,q}^{(m)} - \tilde{p}_{test,q}^{(m)} | / | p_{test,q}^{(m)} |\right)$ is utilized where $p_{test,q}^{(m)}$ and $\tilde{p}_{test,q}^{m}$ are the actual and predicted q-th parameter of the m-th test sample ($m = 1,..., M$) respectively. It is evident from Figure 3, NME is slightly decreasing for h_c estimation with the increment of N and is not effected so much in presence of noise. Even at lower N value and noisy test set (e.g., $SNR = 20$ dB), h_c can be estimated. However, with increasing training samples additively, NME is decreasing significantly for w_c estimation for both noiseless and noisy test cases. That means, groove width (w_c) estimation suffers a lot for lower N and in presence of noisy test set. Consequently, more samples need to be added so as to represent enough impedance variation information due to the variation of w_c. This also helps the learning algorithm (i.e., SVR) to build optimal model for inverse solution. Therefore, the proposed approach uniformly explores the feature space by most significant features (i.e., J=4), and fills the parameter space mostly with higher values of h_c and uniform spacing of w_c [Fig. 2(*b*)].

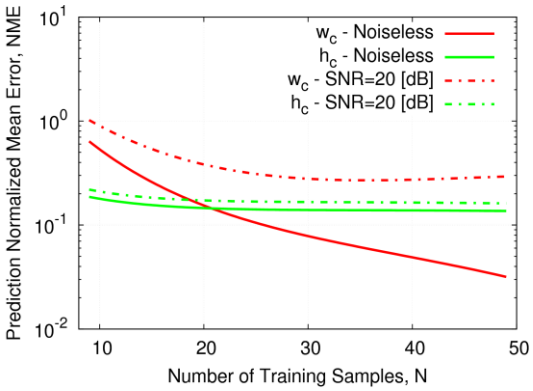

Figure 3. Prediction accuracy in terms of Normalized Mean Error (NME) vs. training size N for noiseless and noisy test set ($SNR = 20$ dB) for J = 4; Q = 2 by *PLS-OSF/SVR*.

In Figure 4, the robustness of *PLS-OSF/SVR* approach on noisy test set for estimating groove parameters is also depicted in terms of actual vs. predicted plots considering a fixed number of training samples (i.e., $N = 49$) and $J = 4$. With increasing noise (i.e., decreasing *SNR* value) on test set, h_c estimation [Fig. 4(a) - Fig. 4(d)] is not effected so much compare to w_c estimation [Fig. 4(e) - Fig. 4(h)]. However, even at noisy environment for a training set of $N = 49$ samples, w_c estimation shows reasonable accuracy (Fig. 3 and Fig. 4) by applying *PLS-OSF/SVR* technique.

The performance comparison between *PLS-OSF/SVR* technique for $J = 4$ and a standard *GRID/SVR* [10] approach is shown in Figure 5 in terms of the actual vs. predicted groove height and width considering the number of training samples $N = 49$. The considered training set for *GRID-SVR* is obtained by a full grid made by 7×7 (i.e., $N = 49$) samples having $F = 2K = 2 \times 73 = 146$ measured features. *PLS-OSF/SVR* shows better prediction accuracy than *GRID/SVR* by showing lower variance among the actual and predicted values (Fig. 5). Moreover, *GRID/SVR* fails to predict h_c and w_c with constant prediction in case of noisy test set that are not shown here (for sake of brevity). Contrarily, the transformation of actual F features into different extracted feature space by PLS makes *PLS-OSF/SVR* strategy more robust on noisy test set (Fig. 3 and Fig. 4).

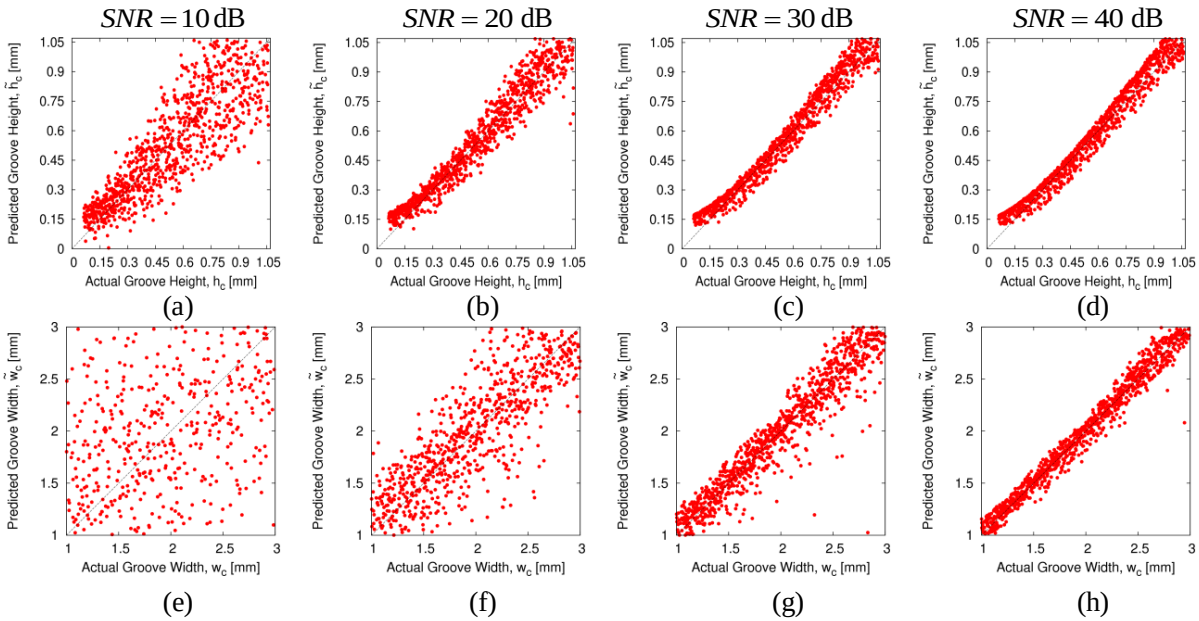

Figure 4. Actual vs. predicted plots for M=1000 test configurations at $SNR = [10, 20, 30, 40]$ dB, when N=49, $J = 4$ for groove (*a*) - (d) height, h_c and (*e*) - (h) width, w_c by *PLS-OSF/SVR*.

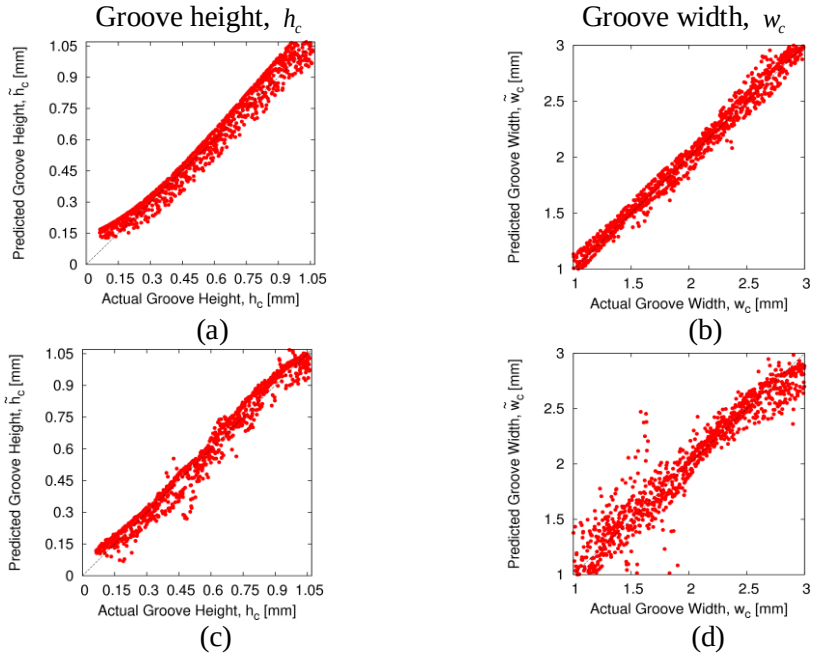

Figure 5. Actual vs. predicted h_c, w_c for M=1000 test configurations at *Noiseless* when N=49 for (*a*) - (b) *PLS-OSF/SVR* and (*c*) - (d) standard *GRID/SVR*.

4. Conclusion

In this work, we have shown an innovative real time inversion solution within the framework of Learning-by-Examples (LBE) for groove characterization in tube structure. PLS feature extraction

combined with OSF sampling has shown the ability to build a more suitable training set than standard approach (i.e., full grid). The estimation accuracy and robustness of *PLS-OSF/SVR* strategy is numerically validated in presence of noisy test set and compared with standard *GRID/SVR* approach on noiseless test set. On the other hand, SVR shows the ability to deal with noisy test set if suitable training set is provided. Moreover, quasi real time inversion has been obtained for testing M=1000 test samples for 0.08s during *offline* phase on a standard laptop.

References

[1] Salucci M, Poli L and Massa A 2017 Advanced multi-frequency GPR data processing for non-linear deterministic imaging *Signal Processing- Special issue on Advanced Ground-Penetrating Radar Signal-Processing Techniques* **132** 306-318
[2] Salucci M, Oliveri G and Massa A 2015 GPR Prospecting through an inverse scattering frequency-hoping multi-focusing approach *IEEE Trans. Geosci. Remote Sens.* **53** 6573-6592
[3] Rocca P, Benedetti M, Donelli M, Franceschini D and Massa A 2009 Evolutionary optimization as applied to inverse problems *Inverse Problems* **25** 1-41
[4] Salucci M, Poli L, Anselmi N and Massa A 2017 Multifrequency particle swarm optimization for enhanced multi-resolution GPR microwave imaging *IEEE Trans. Geosci. Remote Sens.* **55** 1305-1317
[5] Henriksson T, Lambert M and Lesselier D 2011 Non-Iterative MUSIC-Type Algorithm for Eddy-Current Nondestructive Evaluation of Metal Plates *Studies in Applied Electromagnetics and Mechanics: Electromagnetic Nondestructive Evaluation (XIV)* **35** 22-29
[6] Tamburrino A,Vento A,Ventre S and Maffucci A 2016 Monotonicity imaging method for flaw detection in aeronautical applications *Studies in Applied Electromagnetics and Mechanics: Electromagnetic Nondestructive Evaluation (XIX)* **41** 284-292
[7] Douvenot R, Lambert M and Lesselier D 2011 Adaptive metamodels for crack characterization in eddy-current testing *IEEE Trans. Magn.* **47** 746-755
[8] Bilicz S, Lambert M, Gyimóthy S and Pávó J 2012 Solution of Inverse Problems in Nondestructive Testing by a Kriging-Based Surrogate Model *IEEE Trans. Magn.* **48** 495-498
[9] Salucci M, Ahmed S and Massa A 2016 An Adaptive Learning-by-Examples Strategy for Efficient Eddy Current Testing of Conductive Structures *Proc. Conf. EuCAP* **10**
[10] Salucci M, Anselmi N, Oliveri G, Calmon P, Miorelli R, Reboud C and Massa A 2016 Real-Time NDT-NDE Through an Innovative Adaptive Partial Least Squares SVR Inversion Approach *IEEE Trans. Geosci. Remote Sens.* **54** 6818-6832
[11] Wold S, Sjostrom M and Eriksson L 2001 PLS-regression: a basic tool of chemometrics *Chemometrics and Intelligent Laboratory Systems* **58** 109-130
[12] Smola A J and Scholkopf B A tutorial on support vector regression 2004 *Statistics and Computing* **14** 199-222
[13] Lesselier D and Razek A 2002 A Eddy current scattering and inverse scattering: Green's integral and variational formulations *Scattering: Scattering and Inverse Scattering in Pure and Applied Science. Part I. Scattering of Waves by Macroscopic Targets* 486-507
[14] CIVA: Simulation and Analysis for NDT. http://www.civa.cea.fr [Online]

Acknowledgment

This work has been partially supported by the SIRENA project (2014-2017) funded by DIGITEO (France) under the "Call for Chairs 2014" and French project ANR-ByPASS.